

Graphene field-effect transistors with gigahertz-frequency power gain on flexible substrates

Nicholas Petrone[†], Inanc Meric[‡], James Hone[†], and Kenneth L. Shepard^{‡}*

[†]Department of Mechanical Engineering, [‡]Department of Electrical Engineering,

Columbia University, New York, New York 10027, United States

ABSTRACT

The development of flexible electronics operating at radio-frequencies (RF) requires materials that combine excellent electronic performance and the ability to withstand high levels of strain. In this work, we fabricate graphene field-effect transistors (GFETs) on flexible substrates from graphene grown by chemical vapor deposition (CVD). Our devices demonstrate unity-current-gain frequencies, f_T , and unity-power-gain frequencies, f_{max} , up to 10.7 and 3.7 GHz, respectively, with strain limits of 1.75%. These devices represent the only reported technology to achieve gigahertz-frequency power gain at strain levels above 0.5%. As such, they demonstrate the potential of CVD graphene to enable a broad range of flexible electronic technologies which require both high-flexibility and RF operation.

The field of flexible electronics has been active for more than 15 years, driven by the desire for low-cost, large-area, pliable electronics for such applications as e-paper, flexible displays, chemical and biological sensors, and smart tags.¹ The electronic materials used in these cases have largely been polymers and small-molecule organic films because of the desire to exploit large-area, low-cost fabrication approaches, such as roll-to-roll dry² or inkjet printing.³ The resulting electronic device performance, however, has been relatively poor, with inherent low-field mobilities typically less than $1 \text{ cm}^2 \text{ V}^{-1} \text{ s}^{-1}$ and mobilities in integrated devices typically below $0.05 \text{ cm}^2 \text{ V}^{-1} \text{ s}^{-1}$.¹⁻³ Both reliability and low-voltage operation have been challenging. In addition, it is important for any proposed flexible technology to maintain uniform electronic properties over a wide range of strain, ε , which is related to the thickness, t , and bending radius, ρ , of the substrate as $\varepsilon = t/(2\rho)$.

The desire to improve the performance of these devices has led to growing efforts to transfer wires, ribbons, and membranes of traditional semiconducting materials to flexible substrates. Materials such as silicon nanomembranes (SiNMs),⁴⁻⁷ III-V metal-oxide-semiconductor thin-films⁸ and nanowires,⁹ indium-gallium-zinc-oxide,¹⁰ and AlGaIn/GaN heterostructures¹¹ have been investigated, as have carbon nanotubes (CNTs),¹²⁻¹⁵ and graphene.¹⁶⁻¹⁷ However, enhancements to electronic performance have been achieved at the expense of device flexibility; to date, no flexible technology has achieved both unity-current-gain frequencies, f_T , and unity-power-gain frequencies, f_{max} , in the GHz regime at strains above 0.5%. CNT devices have demonstrated f_T performance approaching 1 GHz at 1% strain for 0.8- μm channel lengths.¹²⁻¹³ However, f_{max} , which is far more important for circuit applications, is not reported. In fact, f_{max} is expected to be substantially less than f_T , following similar trends for field-effect transistors (FETs) based on mats of CNTs on rigid substrates.¹⁸ The highest values of f_{max} for FETs

fabricated on flexible substrates have been reported for SiNMs⁵ and III-V metal-oxide-semiconductor thin films⁸ at 12 and 23 GHz, respectively. However, FETs based on these bulk semiconductor materials all exhibit strain limits below 0.5%.^{4-5, 8, 11}

Graphene's unique electronic¹⁹⁻²⁰ and mechanical²¹ properties make it a promising material for the fabrication of FETs which require both high flexibility and high operating frequencies. While graphene has no band-gap, rendering it poorly suited for digital applications, its high carrier mobility,^{19, 22} saturation velocity,²³⁻²⁵ and current-carrying capacity²⁶⁻²⁷ make it a promising candidate for high-frequency analog applications. Graphene-based FETs (GFETs) fabricated on rigid substrates have in fact demonstrated values of f_{\max} of up to 34 GHz at channel lengths of 600 nm.²⁸

Methods for producing graphene films suitable for flexible electronics include dielectrophoretic deposition of solution-processed graphene¹⁶ and large-area growth of graphene by chemical vapor deposition (CVD).²⁹ GFETs from solution-processed methods demonstrate f_T performance of approximately 2.2 GHz at 170-nm channel length under strain up to 0.5%.¹⁶ However, poor electrostatics in these devices result in non-saturating current-voltage ($I - V$) characteristics and f_{\max} values of only 550 MHz.¹⁶ In contrast, CVD graphene films display excellent electronic properties comparable to those of exfoliated graphene.³⁰ Even on flexible substrates, GFETs fabricated from CVD graphene exhibit field-effect mobilities up to $4,900 \text{ cm}^2\text{V}^{-1}\text{s}^{-1}$ ³¹ and maintain stable DC electronic properties at high levels of strain.³²⁻³⁷ In this work we demonstrate GFETs fabricated from CVD graphene with f_{\max} of 3.7 GHz (at channel lengths of 500 nm) and strain limits of 1.75%. Fig. 1 compares the work presented here with other flexible high-frequency technologies on the merits of f_{\max} and strain limits, showing that the GFETs fabricated in this work are the first transistors to attain power gain in the GHz regime at strains above 0.5%.

Fig. 2a shows a schematic of the GFETs fabricated in this work. A bottom-gated device structure is implemented, motivated by previous work demonstrating that bottom-gated fabrication of GFETs with a dielectric layer applied over the gate electrode yields higher performance than top-gated devices which attempt to grow a gate oxide on the graphene surface.^{28, 38} GFETs are fabricated on 127 μm thick polyethylene naphthalate (PEN) substrates (DuPont Teijin Films). Two-fingered bottom-gates (1nm Ti/30nm Au-Pd alloy) are defined by electron beam lithography and lift-off. The contact pad region of the gate is further thickened by subsequent patterning and evaporation of Ti/Au (1nm/50nm). A 6-nm gate dielectric of HfO_2 is conformally grown by atomic layer deposition (ALD) at 150 $^\circ\text{C}$ yielding a dielectric constant of $\kappa \approx 13$.³⁹ Large, single-crystals of graphene are grown by chemical vapor deposition (CVD) and transferred over the gate using well-established procedures.³⁰ Graphene is patterned with a second lithography step and reactive ion etching in an oxygen plasma. The devices are completed by evaporating Ti/Pd/Au (1nm/15nm/50nm) source and drain electrodes to contact the graphene. Devices are left uncapped. In addition, the thermal limits of the polymer substrate (~ 180 $^\circ\text{C}$) prevent high-temperature thermal annealing processes from being used to remove resist residue on the graphene channel. Fig. 2b shows a cross-sectional schematic of a completed device. GFETs are fabricated with a gate length of 500 nm, source-to-drain spacing of 900 nm, and an effective channel width of 30 μm (two 15- μm wide gates in parallel). Fig. 2c shows an optical micrograph of a GFET device fabricated on a PEN substrate.

Electronic device characteristics are measured under ambient conditions. Samples are strained during electronic measurements by applying uniaxial tensile strain in the y-direction (see Fig. 2c) under two-point bending conditions, as shown in Fig. 2d. The strain, ϵ_{yy} , is calculated from the bending geometry using elastica theory assuming frictionless end-supports.⁴⁰

Flexible GFET DC performance in the linear transport region is shown in Figs. 3a-c, where device resistance, R , is displayed against gate-to-source voltage, V_{gs} , taken with fixed source-to-drain voltage ($V_{sd} = 10$ mV) at increasing strain from $\varepsilon_{yy} = 0\%$ to 1.75%. Low-bias field-effect mobility, μ_{FE} , is calculated from $\mu_{FE} = (L_{ch} g_m) / (W_{ch} C_{tot} V_{sd})$, where L_{ch} is the channel length, W_{ch} is the channel width, C_{tot} is the total effective gate capacitance per unit area, and g_m is the small-signal transconductance, defined as $(\partial I_d / \partial V_{gs})|_{V_{sd}}$, where I_d is the measured drain current. C_{tot} is determined by the series combination of the electrostatic capacitance, C_e , and the quantum capacitance, C_q . For the devices presented in this work, $C_e \approx 1700$ nF cm⁻², based on a parallel plate model. C_q is density dependent over the charge carrier density range pertinent to this work ($n = 0.5 - 10 \times 10^{12}$ cm⁻²), but it can be approximated as the mean of C_q values calculated over this carrier density range. This approach, shown to be valid for similar devices over an equivalent carrier density range,⁴¹ yields a constant value of $C_q \approx 2000$ nF cm⁻². These values of C_e and C_q result in $C_{tot} \approx 919$ nF cm⁻². The source-to-gate current, I_{sg} , is measured to remain below 0.5 pA over the entire strain range during device characterization, indicating negligible leakage current through the dielectric even at high strain. μ_{FE} for our flexible GFET is $\sim 1,500$ cm² V⁻¹ s⁻¹ (for $V_{gs} = -0.25$ V, the gate bias that yields the maximum g_m for this device). This mobility is comparable to similar devices fabricated from exfoliated graphene on silicon substrates,^{38, 41} demonstrating the excellent electronic quality of the CVD graphene utilized in this work. Although mobility remains relatively constant with strain up to $\varepsilon_{yy} = 1.75\%$, the position of the Dirac point with respect to V_{gs} is observed to shift with increasing strain. We attribute this shift to changes in device electrostatics, related to mobile trapped charges in the gate-oxide and graphene-oxide interfaces, as the substrate is flexed. The presence of trapped charges in the gate-oxide, at the graphene-oxide interface, or in resist residue on the graphene

surface additionally accounts for the hysteresis in the position of the Dirac point with respect to V_g (~ 0.5 V) observed in low-bias measurements. We note, however, that the presence of residual resist residue from lithographic processing does not significantly contribute to the contact resistance between the graphene channel and evaporated electrodes, as the total contact resistance for this device is less than $300 \Omega\text{-}\mu\text{m}$, in the range best contact resistances reported for GFET devices ($200\text{-}1,000 \Omega\text{-}\mu\text{m}$).⁴¹⁻⁴³ The ungated regions of the graphene channel will, however, effectively increase the contact resistance of the device. Improvements to the device architecture which act to minimize the gate-to-source and gate-to-drain spacer regions, such as by utilizing a self-aligned fabrication scheme, can further reduce the effective channel resistance.

Figs. 3d-f show $I - V$ characteristics for the same representative device, with I_d plotted as a function of V_{sd} at values of V_{gs} decreasing from 0.25 V to -1 V in 0.25 V steps. Device characteristics represent a unipolar p-channel device. Devices are only measured up to $V_{sd} = 0.5$ V due to the thermal limitations of the polymer substrate. Above $V_{sd} = 0.5$ V the substrate melts locally under the device channel, causing both the substrate and overlaying GFET to mechanically warp in structure. $I - V$ characteristics are plotted for increasing levels of strain ranging from 0% to 1.75% . Changes in I_d with increasing strain are correlated to the observed shifts in the Dirac point in Figs. 2a-c. At $\varepsilon_{yy} = 0\%$, measured values of g_m and output resistance, r_o , are 5.1 mS and 259Ω , respectively, at a bias point of $V_{gs} = -0.25$ V and $V_{sd} = 0.5$ V. We observe a maximum current density of 0.28 mA/ μm , consistent with values reported for devices fabricated from CVD graphene of similar structure at equivalent electric fields.^{31, 37, 44}

Fig. 4 shows RF characteristics for this same GFET device characterized in Fig. 3. Both current-gain (h_{21}) and unilateral power gain (U) are extracted from S -parameters measured at $V_{sd} = 0.5$ V. V_{gs} values are chosen to maximize device transconductance; these values change with strain due

to the Dirac point voltage shifts observed in Figs. 3a-c. The device demonstrates extrinsic cut-off frequency values (without any de-embedding) of $f_T = 7.2$ GHz and $f_{\max} = 2.6$ GHz at a bias point of $V_{gs} = -0.25$ V at $\varepsilon_{yy} = 0\%$, as shown in Fig. 4a. At $\varepsilon_{yy} = 1.25\%$, $f_T = 10.7$ GHz and $f_{\max} = 3.7$ GHz are observed at $V_{gs} = 0.4$ V (Fig. 4b). The RF performance does not degrade from its unstrained values up to strains of $\varepsilon_{yy} = 1.75\%$ (Fig. 4c). We note that previously mentioned restrictions on the range of applied V_{sd} , resulting from thermal constraints of the polymer substrate, prevent strong current saturation and ultimately limit f_{\max} performance.²⁸ In spite of these limitations, these devices yield comparable performance to GFETs fabricated on rigid substrates with a similar layout.⁴⁵

Fig. 5 shows the evolution of relevant device parameters with strain. Fig. 5a-d plot DC characteristics as a function of strain. Both g_m (Fig. 5a) and r_o (Fig. 5b) exhibit low variance (less than $\pm 25\%$) up to strains of $\varepsilon_{yy} = 1.1\%$. At strains greater than 1.1%, variations in r_o increase up to $\pm 40\%$, likely related to the observed shifts in device electrostatics (most notably the shift in the Dirac point) with flexure. Fig. 5c plots device gate capacitance extracted directly from measured scattering parameters, C_g , as a function of strain. We note that the value of C_g extracted at $\varepsilon_{yy} = 0\%$ is 941 nF cm^{-2} , which matches well the expected value for C_{tot} of 919 nF cm^{-2} as described before. The variation in C_g with strain is likely attributed to aforementioned shifts in trapped charges. Accounting for observed variations in C_g with strain, values of μ_{FE} at strains above $\varepsilon_{yy} = 0\%$ are calculated utilizing C_g values extracted at equivalent strain states. Mobility for the device remains uniform with device flexure (Fig. 5d), exhibiting less than $\pm 30\%$ variance across the entire measured strain range up to $\varepsilon_{yy} = 1.75\%$, in good agreement with previous theoretical calculations⁴⁶ and experimental observations,⁴⁷ demonstrating the stability of the intrinsic electronic properties of the CVD graphene channel. Figs. 5e,f plot cut-off frequency

as a function of strain. In all cases, V_{sd} is 0.5 V and V_{gs} is chosen at each measured strain point to maximize the device transconductance; these values of V_{gs} are also shown in Fig. 5e. Both f_T and f_{max} demonstrate low variance (less than $\pm 20\%$) with strain up to $\varepsilon_{yy} = 1.1\%$, above which an increase in both f_T and f_{max} of up to 40% is observed. We note that both DC and RF performance of the device remain uniform up to strains of $\varepsilon_{yy} = 1.1\%$; improvements to device structure which reduce trapped charges can allow for improved uniformity of electronic properties at strains greater than $\varepsilon_{yy} = 1.1\%$. Above strains of $\varepsilon_{yy} = 1.75\%$, most devices begin to fail as a result of cracking of the gate electrode, corresponding to clear irreversible degradations in electronic characteristics.

In conclusion, we demonstrate flexible GFETs fabricated from CVD graphene which display extrinsic values of f_T and f_{max} up to 10.7 GHz and 3.7 GHz, respectively, with strain limits of 1.75%. This is the first example of a flexible technology exhibiting both gigahertz-frequency power gain and strain limits above 0.5%. As such, this work demonstrates the potential of CVD graphene as a material to enable a wide-range of highly-flexible electronic technologies requiring analog FETs operating in the gigahertz frequency range.

FIGURES

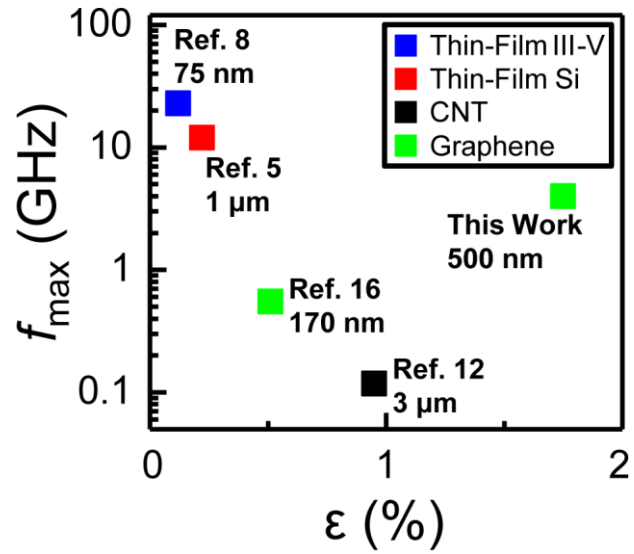


Figure 1. Comparison of f_{\max} and strain limits of flexible FET technologies. Channel lengths of the associated devices yielding these performances are noted.

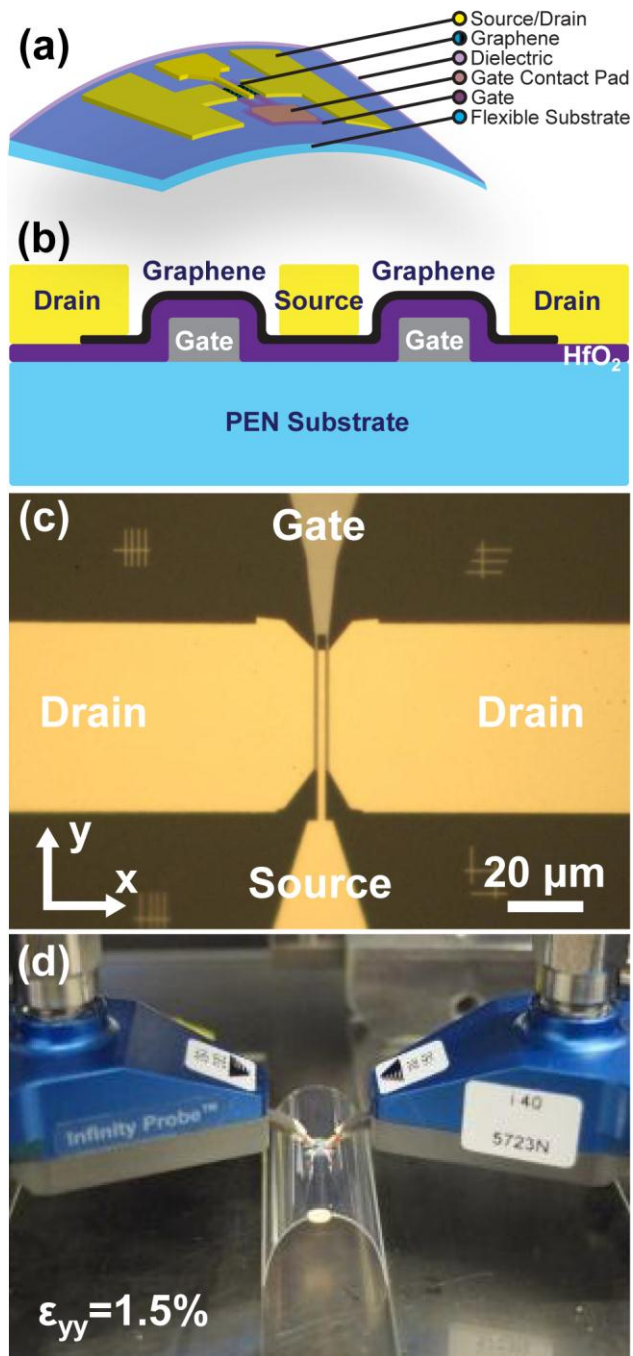


Figure 2. (a) Schematic of GFET fabricated on PEN, a flexible and transparent substrate. (b) Cross-sectional schematic of flexible GFET device. (c) Optical micrograph of GFET fabricated with a gate length of 500 nm and a source-to-drain spacing of 900 nm. (d) Photograph of electronic measurement approach for GFET under 1.5% strain.

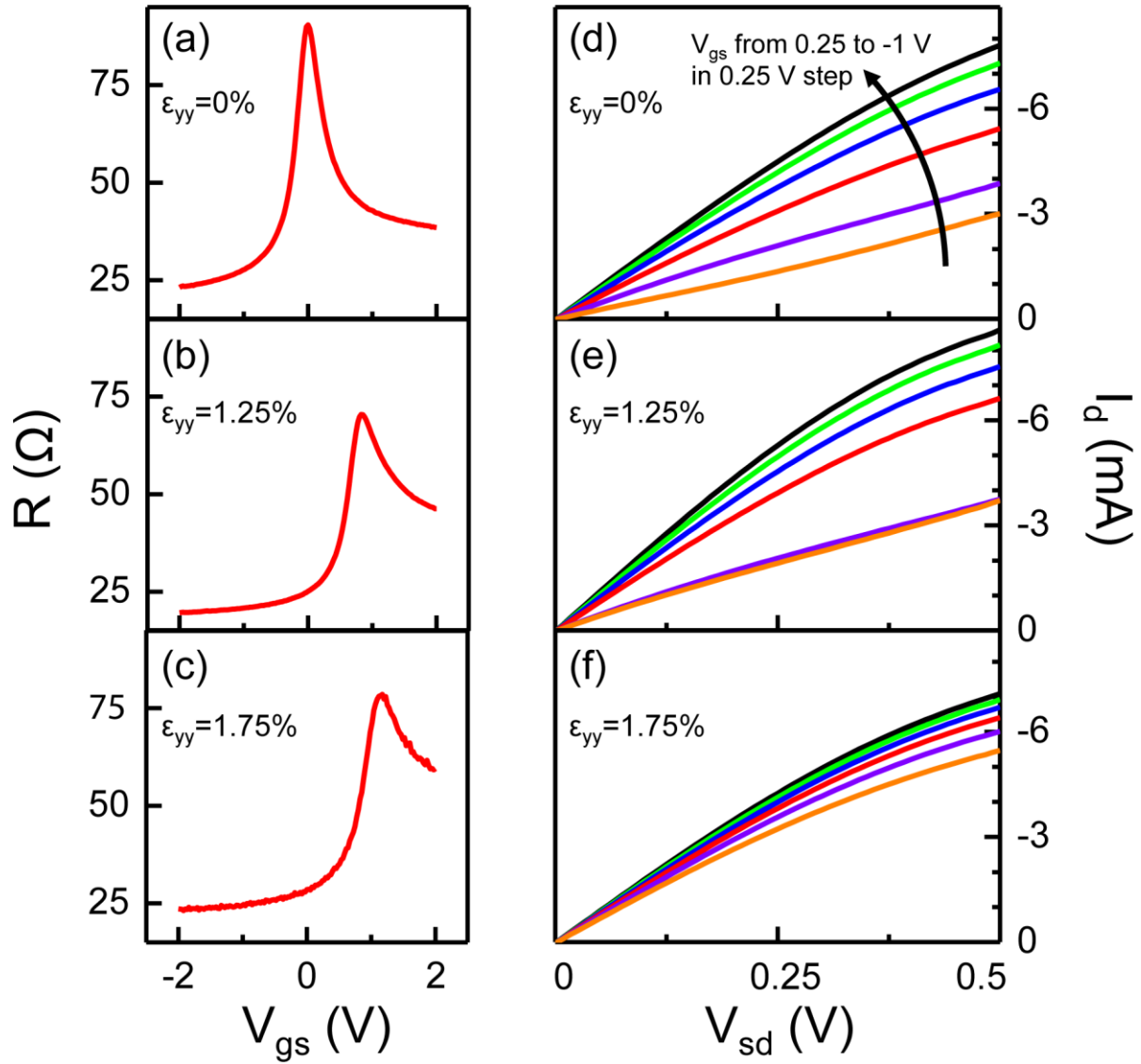


Figure 3. (a-c) Low-field transport characteristics of a flexible GFET with a device channel width of $30\ \mu\text{m}$. Device resistance, R , is plotted against gate-to-source voltage, V_{gs} , at a fixed source-to-drain bias of $V_{sd} = 10\ \text{mV}$. (d-f) Current-voltage ($I - V$) characteristics plotting drain current, I_d , as a function of V_{sd} . $I - V$ curves are taken at fixed V_{gs} decreasing from $0.25\ \text{V}$ (orange) to $-1\ \text{V}$ (black) in $0.25\ \text{V}$ steps. Data are presented for increasing values of strain of $\epsilon_{yy} = 0\%$ (a,d), $\epsilon_{yy} = 1.25\%$ (b,e), and $\epsilon_{yy} = 1.75\%$ (c,f).

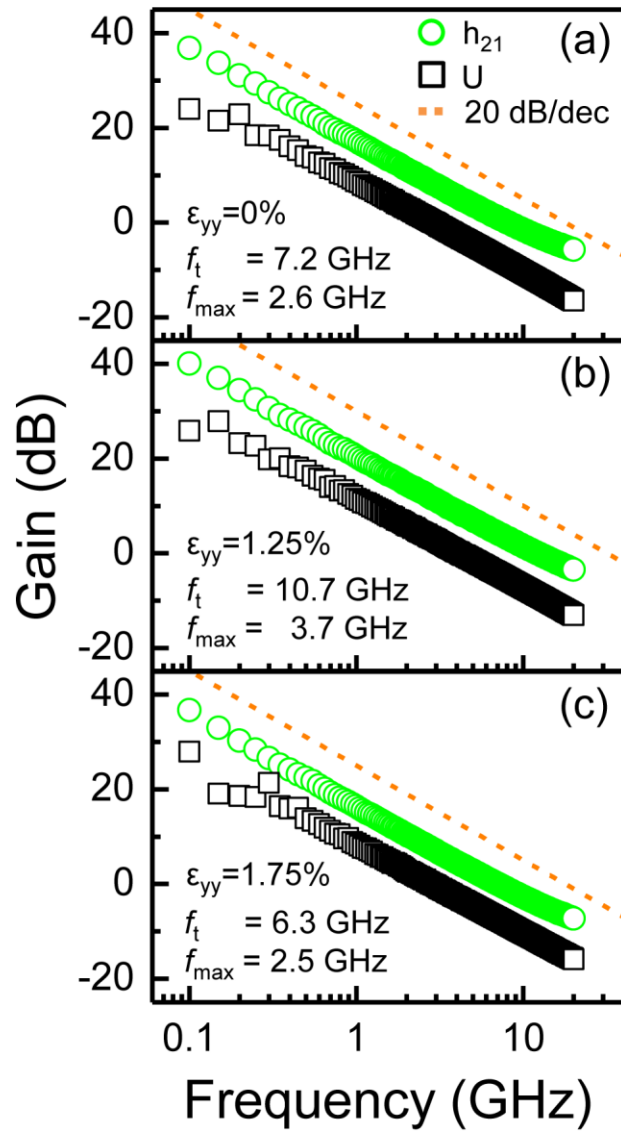


Figure 4. High-frequency device characteristics, current gain (h_{21}) and unilateral power gain (U), plotted as a function of frequency (without de-embedding). High-frequency characteristics are presented for strain values of $\epsilon_{yy} = 0\%$ (a), $\epsilon_{yy} = 1.25\%$ (b), and $\epsilon_{yy} = 1.75\%$ (c). Values of extrinsic f_T and f_{max} are calculated for each strain state. Measurements are performed at a fixed source-to-drain voltage, V_{sd} , of 0.5 V and gate-to-source voltages, V_{gs} , of -0.25 V (a), 0.4 V (b), and 0.6 V (c). The dashed line is a guide to the eye with a -20 dB/decade slope, included to demonstrate that devices follow well this expected frequency dependence.

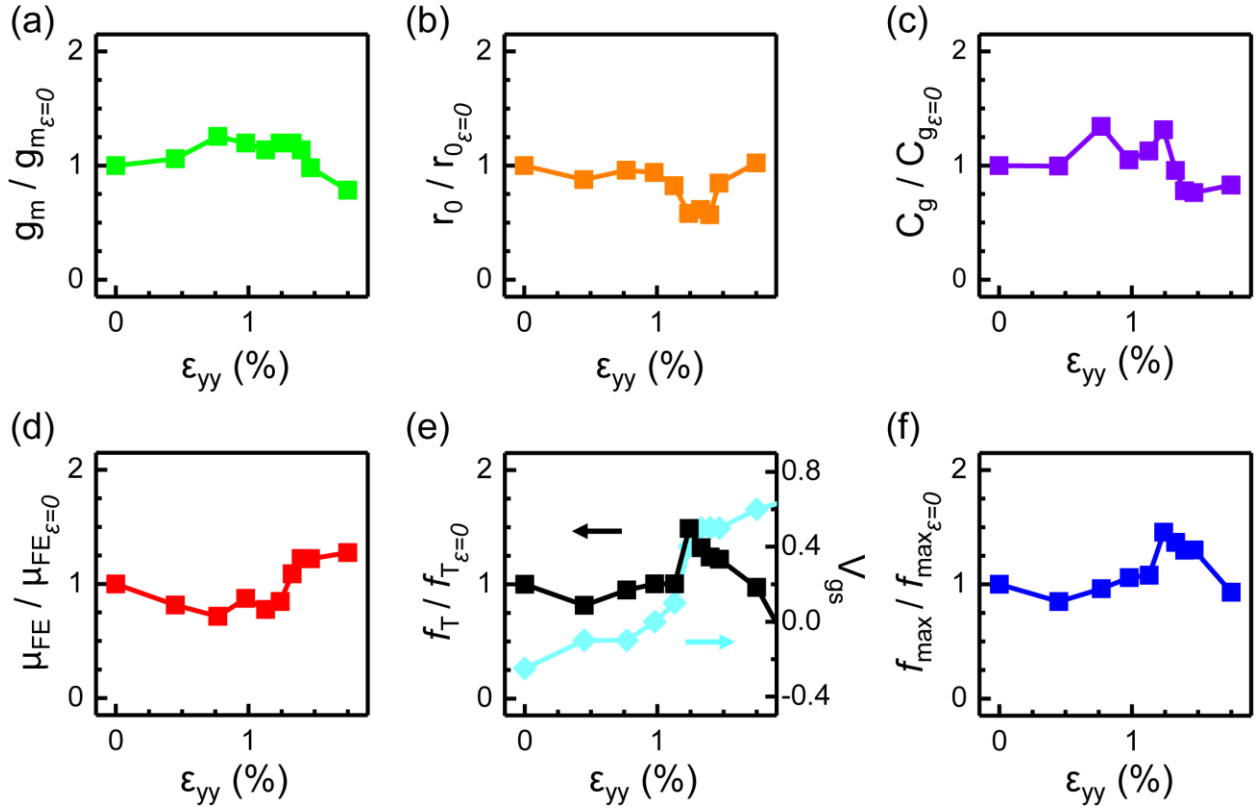


Figure 5. Device characteristics, normalized by their zero-strain values, plotted as a function of strain, ϵ_{yy} . Data is presented for (a) maximum transconductance, g_m ; (b) maximum output resistance, r_o ; (c) gate capacitance, C_g ; (d) field-effect mobility, μ_{FE} ; (e) unity-current-gain frequency, f_T , (black) and the corresponding gate-to-source bias, V_{gs} , used to maximize transconductance (light blue); and (f) unity-power-gain frequency, f_{max} .

CORRESPONDING AUTHOR

*E-mail: shepard@ee.columbia.edu

FUNDING SOURCES

This work was funded by the Office of Naval Research under contract N00014-1210814, by the AFOSR MURI Program on new graphene materials technology, and by the Focus Center Research Program C2S2 Center.

ACKNOWLEDGMENT

N.P. thanks Prof. Jeffrey W. Kysar, Dr. Cory R. Dean, Dr. Gwan Hyoung Lee, and Dr. Arend M. van der Zande for helpful discussions.

REFERENCES

1. Ananth, D. Organic and polymer transistors for electronics. *Materials Today* **2006**, 9 (4), 24-30.
2. Blanchet, G. B.; Loo, Y. L.; Rogers, J. A.; Gao, F.; Fincher, C. R. Large area, high resolution, dry printing of conducting polymers for organic electronics. *Appl Phys Lett* **2003**, 82 (3), 463-465.
3. Sirringhaus, H.; Kawase, T.; Friend, R. H.; Shimoda, T.; Inbasekaran, M.; Wu, W.; Woo, E. P. High-resolution inkjet printing of all-polymer transistor circuits. *Science* **2000**, 290 (5499), 2123-2126.
4. Qin, G. X.; Yuan, H. C.; Celler, G. K.; Ma, J. G.; Ma, Z. Q. Influence of bending strains on radio frequency characteristics of flexible microwave switches using single-crystal silicon nanomembranes on plastic substrate. *Appl Phys Lett* **2011**, 99 (15).
5. Sun, L.; Qin, G. X.; Seo, J. H.; Celler, G. K.; Zhou, W. D.; Ma, Z. Q. 12-GHz Thin-Film Transistors on Transferrable Silicon Nanomembranes for High-Performance Flexible Electronics. *Small* **2010**, 6 (22), 2553-2557.
6. Yuan, H. C.; Celler, G. K.; Ma, Z. Q. 7.8-GHz flexible thin-film transistors on a low-temperature plastic substrate. *J Appl Phys* **2007**, 102 (3).
7. des Etangs-Levallois, A. L.; Dubois, E.; Lesecq, M.; Danneville, F.; Poulain, L.; Tagro, Y.; Lepilliet, S.; Gloria, D.; Raynaud, C.; Troadec, D. 150-GHz RF SOI-CMOS Technology in Ultrathin Regime on Organic Substrate. *IEEE Electron Device Lett* **2011**, 32 (11), 1510-1512.
8. Wang, C.; Chien, J. C.; Fang, H.; Takei, K.; Nah, J.; Plis, E.; Krishna, S.; Niknejad, A. M.; Javey, A. Self-Aligned, Extremely High Frequency III–V Metal-Oxide-Semiconductor Field-Effect Transistors on Rigid and Flexible Substrates. *Nano Lett* **2012**, 12 (8), 4140-4145.
9. Takahashi, T.; Takei, K.; Adabi, E.; Fan, Z. Y.; Niknejad, A. M.; Javey, A. Parallel Array InAs Nanowire Transistors for Mechanically Bendable, Ultrahigh Frequency Electronics. *ACS Nano* **2010**, 4 (10), 5855-5860.
10. Kinkeldei, T.; Munzenrieder, N.; Zysset, C.; Cherenack, K.; Troster, G. Encapsulation for Flexible Electronic Devices. *IEEE Electron Device Lett* **2011**, 32 (12), 1743-1745.
11. Lesecq, M.; Hoel, V.; des Etangs-Levallois, A. L.; Pichonat, E.; Douvry, Y.; De Jaeger, J. C. High Performance of AlGaN/GaN HEMTs Reported on Adhesive Flexible Tape. *IEEE Electron Device Lett* **2011**, 32 (2), 143-145.
12. Wang, C.; Chien, J. C.; Takei, K.; Takahashi, T.; Nah, J.; Niknejad, A. M.; Javey, A. Extremely Bendable, High-Performance Integrated Circuits Using Semiconducting Carbon Nanotube Networks for Digital, Analog, and Radio-Frequency Applications. *Nano Lett* **2012**, 12 (3), 1527-1533.
13. Chimot, N.; Derycke, V.; Goffman, M. F.; Bourgoin, J. P.; Happy, H.; Dambrine, G. Gigahertz frequency flexible carbon nanotube transistors. *Appl Phys Lett* **2007**, 91 (15).
14. Vaillancourt, J.; Zhang, H. Y.; Vasinajindakaw, P.; Xia, H. T.; Lu, X. J.; Han, X. L.; Janzen, D. C.; Shih, W. S.; Jones, C. S.; Stroder, M.; Chen, M. Y. H.; Subbaraman, H.; Chen, R. T.; Berger, U.; Renn, M. All ink-jet-printed carbon nanotube thin-film transistor on a polyimide substrate with an ultrahigh operating frequency of over 5 GHz. *Appl Phys Lett* **2008**, 93 (24).
15. Cao, Q.; Kim, H. S.; Pimparkar, N.; Kulkarni, J. P.; Wang, C. J.; Shim, M.; Roy, K.; Alam, M. A.; Rogers, J. A. Medium-scale carbon nanotube thin-film integrated circuits on flexible plastic substrates. *Nature* **2008**, 454 (7203), 495-U4.

16. Sire, C.; Ardiaca, F.; Lepilliet, S.; Seo, J. W.; Hersam, M. C.; Dambrine, G.; Happy, H.; Derycke, V. Flexible gigahertz transistors derived from solution-based single-layer graphene. *Nano Lett* **2012**, *12* (3), 1184-8.
17. Nayfeh, O. M. Graphene Transistors on Mechanically Flexible Polyimide Incorporating Atomic-Layer-Deposited Gate Dielectric. *IEEE Electron Device Lett* **2011**, *32* (10), 1349-1351.
18. Nougaret, L.; Happy, H.; Dambrine, G.; Derycke, V.; Bourgoin, J. P.; Green, A. A.; Hersam, M. C. 80 GHz field-effect transistors produced using high purity semiconducting single-walled carbon nanotubes. *Appl Phys Lett* **2009**, *94* (24), 243505.
19. Novoselov, K. S.; Geim, A. K.; Morozov, S. V.; Jiang, D.; Zhang, Y.; Dubonos, S. V.; Grigorieva, I. V.; Firsov, A. A. Electric field effect in atomically thin carbon films. *Science* **2004**, *306* (5696), 666-669.
20. Geim, A. K.; Novoselov, K. S. The Rise of Graphene. *Nat Mater* **2007**, *6*, 183.
21. Lee, C.; Wei, X. D.; Kysar, J. W.; Hone, J. Measurement of the elastic properties and intrinsic strength of monolayer graphene. *Science* **2008**, *321* (5887), 385-388.
22. Zhang, Y. B.; Tan, Y. W.; Stormer, H. L.; Kim, P. Experimental observation of the quantum Hall effect and Berry's phase in graphene. *Nature* **2005**, *438* (7065), 201-204.
23. Akturk, A.; Goldsman, N. Electron transport and full-band electron-phonon interactions in graphene. *J Appl Phys* **2008**, *103* (5).
24. Shishir, R. S.; Ferry, D. K. Velocity saturation in intrinsic graphene. *J Phys-Condens Mat* **2009**, *21* (34).
25. Barreiro, A.; Lazzeri, M.; Moser, J.; Mauri, F.; Bachtold, A. Transport Properties of Graphene in the High-Current Limit. *Phys Rev Lett* **2009**, *103*, 76601.
26. Behnam, A.; Lyons, A. S.; Bae, M. H.; Chow, E. K.; Islam, S.; Neumann, C. M.; Pop, E. Transport in Nanoribbon Interconnects Obtained from Graphene Grown by Chemical Vapor Deposition. *Nano Lett* **2012**, *12* (9), 4424-4430.
27. Yu, J.; Liu, G. X.; Sumant, A. V.; Goyal, V.; Balandin, A. A. Graphene-on-Diamond Devices with Increased Current-Carrying Capacity: Carbon sp(2)-on-sp(3) Technology. *Nano Lett* **2012**, *12* (3), 1603-1608.
28. Meric, I.; Dean, C. R.; Han, S. J.; Wang, L.; Jenkins, K. A.; Hone, J.; Shepard, K. L. High-frequency performance of graphene field effect transistors with saturating IV-characteristics *IEEE International Electron Devices Meeting (IEDM)* **2011**, 2.1.1 - 2.1.4
29. Bae, S.; Kim, H.; Lee, Y.; Xu, X. F.; Park, J. S.; Zheng, Y.; Balakrishnan, J.; Lei, T.; Kim, H. R.; Song, Y. I.; Kim, Y. J.; Kim, K. S.; Ozyilmaz, B.; Ahn, J. H.; Hong, B. H.; Iijima, S. Roll-to-roll production of 30-inch graphene films for transparent electrodes. *Nat Nanotechnol* **2010**, *5* (8), 574-578.
30. Petrone, N.; Dean, C. R.; Meric, I.; van der Zande, A. M.; Huang, P. Y.; Wang, L.; Muller, D.; Shepard, K. L.; Hone, J. Chemical Vapor Deposition-Derived Graphene with Electrical Performance of Exfoliated Graphene. *Nano Lett* **2012**, *12* (6), 2751-2756.
31. Lee, J.; Tao, L.; Hao, Y.; Ruoff, R. S.; Akinwande, D. Embedded-gate graphene transistors for high-mobility detachable flexible nanoelectronics. *Appl Phys Lett* **2012**, *100* (15).
32. Kim, K. S.; Zhao, Y.; Jang, H.; Lee, S. Y.; Kim, J. M.; Kim, K. S.; Ahn, J. H.; Kim, P.; Choi, J. Y.; Hong, B. H. Large-scale pattern growth of graphene films for stretchable transparent electrodes. *Nature* **2009**, *457* (7230), 706-710.
33. Park, J. U.; Nam, S.; Lee, M. S.; Lieber, C. M. Synthesis of monolithic graphene-graphite integrated electronics. *Nat Mater* **2012**, *11* (2), 120-125.

34. Lee, S. K.; Kim, B. J.; Jang, H.; Yoon, S. C.; Lee, C.; Hong, B. H.; Rogers, J. A.; Cho, J. H.; Ahn, J. H. Stretchable Graphene Transistors with Printed Dielectrics and Gate Electrodes. *Nano Lett* **2011**, *11* (11), 4642-4646.
35. Lee, S. K.; Jang, H. Y.; Jang, S.; Choi, E.; Hong, B. H.; Lee, J.; Park, S.; Ahn, J. H. All Graphene-Based Thin Film Transistors on Flexible Plastic Substrates. *Nano Lett* **2012**, *12* (7), 3472-3476.
36. Kim, B. J.; Jang, H.; Lee, S. K.; Hong, B. H.; Ahn, J. H.; Cho, J. H. High-Performance Flexible Graphene Field Effect Transistors with Ion Gel Gate Dielectrics. *Nano Lett* **2010**, *10* (9), 3464-3466.
37. Lu, C. C.; Lin, Y. C.; Yeh, C. H.; Huang, J. C.; Chiu, P. W. High Mobility Flexible Graphene Field-Effect Transistors with Self-Healing Gate Dielectrics. *ACS Nano* **2012**, *6* (5), 4469-4474.
38. Meric, I.; Dean, C. R.; Young, A. F.; Baklitskaya, N.; Tremblay, N. J.; Nuckolls, C.; Kim, P.; Shepard, K. L. Channel Length Scaling in Graphene Field-Effect Transistors Studied with Pulsed Current-Voltage Measurements. *Nano Lett* **2011**, *11* (3), 1093-1097.
39. Farmer, D. B.; Chiu, H. Y.; Lin, Y. M.; Jenkins, K. A.; Xia, F. N.; Avouris, P. Utilization of a Buffered Dielectric to Achieve High Field-Effect Carrier Mobility in Graphene Transistors. *Nano Lett* **2009**, *9* (12), 4474-4478.
40. Scarpello, G. M.; Ritelli, D. Elliptic integral solutions of spatial elastica of a thin straight rod bent under concentrated terminal forces. *Meccanica* **2006**, *41* (5), 519-527.
41. Meric, I.; Han, M. Y.; Young, A. F.; Ozyilmaz, B.; Kim, P.; Shepard, K. L. Current saturation in zero-bandgap, topgated graphene field-effect transistors. *Nat Nanotechnol* **2008**, *3* (11), 654-659.
42. Meric, I.; Dean, C.; Young, A.; Hone, J.; Kim, P.; Shepard, K. L. Graphene field-effect transistors based on boron nitride gate dielectrics. *IEEE International Electron Devices Meeting (IEDM)* **2010**, 23.2.1 - 23.2.4
43. Xia, F. N.; Perebeinos, V.; Lin, Y. M.; Wu, Y. Q.; Avouris, P. The origins and limits of metal-graphene junction resistance. *Nat Nanotechnol* **2011**, *6* (3), 179-184.
44. Wu, Y. Q.; Lin, Y. M.; Bol, A. A.; Jenkins, K. A.; Xia, F. N.; Farmer, D. B.; Zhu, Y.; Avouris, P. High-frequency, scaled graphene transistors on diamond-like carbon. *Nature* **2011**, *472* (7341), 74-78.
45. Han, S. J.; Jenkins, K. A.; Garcia, A. V.; Franklin, A. D.; Bol, A. A.; Haensch, W. High-Frequency Graphene Voltage Amplifier. *Nano Lett* **2011**, *11* (9), 3690-3693.
46. Castro, E. V.; Ochoa, H.; Katsnelson, M. I.; Gorbachev, R. V.; Elias, D. C.; Novoselov, K. S.; Geim, A. K.; Guinea, F. Limits on Charge Carrier Mobility in Suspended Graphene due to Flexural Phonons. *Phys Rev Lett* **2010**, *105* (26).
47. Huang, M. Y.; Pascal, T. A.; Kim, H.; Goddard, W. A.; Greer, J. R. Electronic-Mechanical Coupling in Graphene from in situ Nanoindentation Experiments and Multiscale Atomistic Simulations. *Nano Lett* **2011**, *11* (3), 1241-1246.